Title: Photometry of Three Variable Stars Classified as Pulsators by the ATLAS Survey

Kaelyn Clement

A senior thesis submitted to the faculty of
Brigham Young University
in partial fulfillment of the requirements for the degree of

Bachelor of Science

Eric Hintz, Advisor

Department of Physics and Astronomy

Brigham Young University

ABSTRACT

Title: Photometry of Three Variable Stars Classified as Pulsators by the ATLAS Survey

Kaelyn Clement
Department of Physics and Astronomy, BYU
Bachelor of Science

We have observed three stars classified as potentially multiperiodic pulsating variables under the Asteroid Terrestrial-impact Last Alert System (ATLAS) as part of our variable star follow-up program: HD 357361 (MATLAS 7), ATO J134.0420+42.7679 (MATLAS 14), and ATO J177.8411+10.2881 (MATLAS 69). Using the telescopes at Brigham Young University (BYU), we obtained and processed photometric data in the visual wavelength range. We also obtained archival data from the Transiting Exoplanet Survey Satellite (TESS), the All-Sky Automated Search for Supernovae (ASAS-SN), and from ATLAS itself. We found times of maximum light in order to calculate pulsation periods for each star. These periods agree up to five significant figures with the periods published by ASAS-SN. We also performed Fourier analysis to determine whether each star is multiperiodic. Our analysis of the data agrees with the classification of MATLAS 7 by ASAS-SN as a high-amplitude δ Scuti star. MATLAS 14 does not appear to be a δ Scuti star as classified by ASAS-SN; it is most likely a contact eclipsing binary similar to MATLAS 69 with double the published period. While MATLAS 69 is classified as a pulsator by ATLAS, it is most likely a W Ursae Majoris-type binary as classified by ASAS-SN. Because we used several data sets from different surveys, we were able to examine how varying observation frequencies affected our Fourier analysis and period solutions.

Keywords: [1]Delta Scuti variable stars (370), Multi-periodic variable stars (1079), Pulsating variable stars (1307), W Ursae Majoris variable stars (1783), CCD photometry (208), Asteroseismology (73), Stellar photometry (1620), Optical astronomy (1776), Time series analysis (1916), Light curves (918), Period search (1955), Period determination (1211)

[1]Concepts from the Unified Astronomy Thesaurus (https://astrothesaurus.org/).

ACKNOWLEDGMENTS

I would like to thank my advisor, Dr. Eric Hintz, for this research opportunity and his continued guidance and support on this project. I would also like to thank fellow researcher Christian Suggs for her previous work on the project, which has been a helpful guide for my own work.

We acknowledge the Brigham Young University Department of Physics and Astronomy for their continued support of our research efforts. We acknowledge the Theodore Dunham, Jr. Grant for Research which has been used to help equip the BYU campus observatory. This research was also supported in part by NASA through the American Astronomical Society's Small Research Grant Program.

This research has made use of the SIMBAD database and the "Aladin sky atlas" developed at CDS, Strasbourg, France.

This paper includes data collected by the TESS mission. Funding for the TESS mission is provided by the NASA's Science Mission Directorate.

This work has also made use of data from the European Space Agency (ESA) mission *Gaia* (https://www.cosmos.esa.int/gaia), processed by the *Gaia* Data Processing and Analysis Consortium (DPAC, https://www.cosmos.esa.int/web/gaia/dpac/consortium). Funding for the DPAC has been provided by national institutions, in particular the institutions participating in the *Gaia* Multilateral Agreement.

This work made use of Astropy (http://www.astropy.org): a community-developed core Python package and an ecosystem of tools and resources for astronomy, and Peranso (www.peranso.com), a light curve and period analysis software.

Contents

List of Figures

List of Tables

Chapter 1

Introduction

A star is most stable when it is burning hydrogen in its core. This period of a star's lifetime is called the main sequence and is easily identified when plotted on a temperature vs. intrinsic brightness graph, more commonly known as a Hertzsprung-Russell (H-R) diagram. Once a star exhausts its core hydrogen fuel and begins to burn helium, it becomes unstable, causing layers of the star to expand and/or contract. These changes in the size of the star lead to changes in brightness and temperature which are often periodic in nature.

Astronomers sort these so-called periodic variable stars into groups based on the speed and amplitude of their oscillations. One such group is δ Scuti variable stars, A and F type stars which are located in a turn-off from the main sequence known as the δ Scuti instability strip, shown in Figure 1.1. This is near to the famous Cepheid instability strip, Cepheids being the first group of variable stars to be identified because of their large-amplitude oscillations (Leavitt & Pickering 1912). Although the amplitude of δ Scuti pulsations is not quite as dramatic, they pulsate with shorter periods generally between 0.02 and 0.25 d (Breger 2000). Because these variations occur on such short timescales, we can study these stars more easily than those that vary over weeks, months, or even years. Astronomers can then use these observations to develop a theory of the pulsation mechanisms within the stellar interior in a field known as asteroseismology.

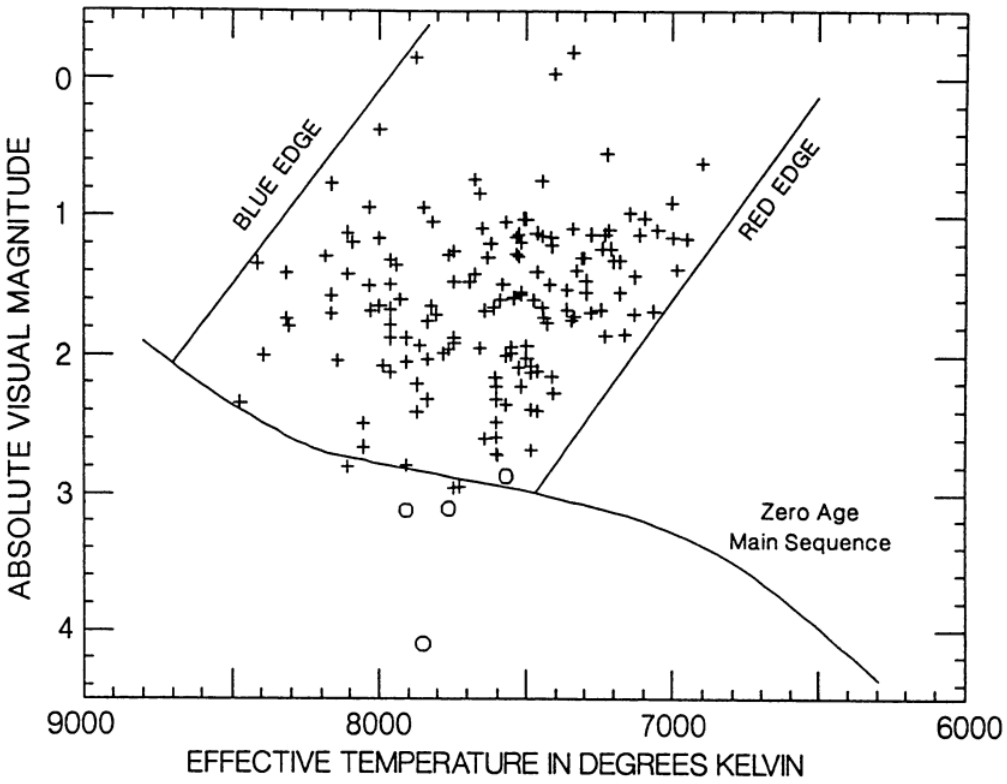

Figure 1.1 H-R diagram of the δ Scuti instability strip, with Population I stars plotted as crosses and Pop. II stars plotted as open circles. From Figure 1 in (Breger 1990).

As with Cepheids, it is believed that δ Scuti stars obey a period-luminosity (P-L) relation, which states that their intrinsic brightness is directly proportional to the log of the period. Thus, knowing the period and apparent magnitude of a certain star, one can calculate the absolute magnitude and determine its distance. The P-L relation is an extremely useful tool in mapping out the structure of the galaxy and beyond. For δ Scuti stars, the P-L relation is still not rigorously defined, and there are different equations for fundamental versus higher-order harmonic pulsators (Poro et al. 2021). Thus, it is necessary to use other methods to find the order of pulsation (see section 3.3).

If a star does not conform well with existing P-L relations, then it may not be a δ Scuti star. There are other types of variable stars that produce light curves resembling δ Scuti stars. These often fit within the broader class of RR Lyrae stars, which form the bridge between δ Scuti and classical Cepheids. One type of star closely related to the δ Scuti class is the γ Doradus star. These stars are typically colder with lower frequencies closer to 1 c/d, but it may be possible for a star to have both δ Scuti- and γ Doradus-type variability (Breger & Beichbuchner 1996).

Another type of star which closely mimics a δ Scuti light curve is the W Ursae Majoris-type binary. These stars do not technically pulsate. Rather, their variability is due to two stars with nearly identical temperature which orbit each other so closely that they share a convective envelope (Lucy 1968). As such, their primary and secondary minima are nearly indistinguishable, and their periods are short enough to fit within the δ Scuti range. In order to distinguish these types of stars from one another, it is necessary to use data such as temperature, surface gravity, stellar extinction, and distance in conjunction with photometric light curves. The best place to start is with a large amount of photometric data; if we can observe the pulsations more frequently, we can calculate a more accurate period for the star.

1.1 Alternate Uses for Transient Event Surveys

Transient event surveys are large-scale observing campaigns that are dedicated to finding specific phenomena occurring in space. However, these surveys have scientific uses beyond their original purpose. In this research, we obtained archival data from three different surveys in order to study multiperiodic variable stars.

The first survey we used is the Asteroid Terrestrial-impact Last Alert System (ATLAS), a project which uses four ground-based telescopes to warn of asteroids that could potentially hit Earth (Heinze et al. 2018). It was funded by NASA and developed by the University of Hawaii. Beyond that, it also processes data related to multiple transient events, including variable stars. The stars studied as part of this research project were classified as pulsators by the ATLAS survey and put on a list for BYU to observe.

Like ATLAS, the All-Sky Automated Survey for Supernovae (ASAS-SN) has also been used to study transient phenomena. This consists of 24 ground-based telescopes whose primary purpose is to detect supernovae (Shappee et al. 2014). It boasts an extensive variable star database with specific classifications. Two of our stars are classified there as δ Scuti stars, while the other is classified as an eclipsing binary.

While ATLAS and ASAS-SN are ground-based, the Transiting Exoplanet Survey Satellite (TESS) is a space-based telescope which surveys large fields of the sky to search for evidence of planets orbiting other stars (Ricker et al. 2015). It has covered nearly all of the sky in long continuous observing periods with three different exposure times (30 minutes, 10 minutes, and 2 minutes). Because it is a space telescope, there is no photometric interference from the atmosphere, although there can be problems with the sun. Because of this, TESS data is extremely useful in studying variable stars with its sheer amount of data. One issue, however, is that TESS uses its own filter system, so light curves cannot be magnitude solved like they are with ATLAS, ASAS-SN, and BYU's own data; as a result, no absolute magnitude can be found.

Table 1.1. Target star IDs and positions

BYU ID	ID	Right Ascension	Declination
MATLAS 7	HD 357361	20:19:25.533	+10:06:52.344
MATLAS 14	ATO J134.0420+42.7679	08:56:10.110	+42:46:04.962
MATLAS 69	ATO J177.8411+10.2881	11:51:21.861	+10:17:17.643

1.2 Stars Analyzed

This work focuses on three specific stars classified as potentially multiperiodic pulsators by ATLAS. We refer to them in this paper by their internal designations of MATLAS 7, MATLAS 14, and MATLAS 69. Their official names and coordinates are summarized in Table 1.1. The goal of this research is to check the published classifications of each star and establish a baseline for calculating the period(s) of each star. We also set out to determine the usefulness of different surveys in analyzing variable stars.

MATLAS 7 is classified as a high-amplitude δ Scuti (HADS) star by ASAS-SN (Jayasinghe et al. 2019). MATLAS 14 is given the designation of δ Scuti (Jayasinghe et al. 2021). However, MATLAS 69 is classified as a W Ursae Majoris-Type Binary (sometimes called WUma), which is not technically a pulsating star, but its light curve closely resembles confirmed pulsators (Jayasinghe et al. 2021). We find that MATLAS 7 is indeed a HADS star and is a double-mode fundamental pulsator with radial oscillations. We find that MATLAS 14 may be too cold to be a δ Scuti star but rather may belong to the W Ursae Majoris class like MATLAS 69. We also tentatively reaffirm the classification of MATLAS 69, with the condition that the stars may be exchanging mass, resulting in variation of the primary and secondary eclipse depths.

In Chapter 2 we will describe the process of collecting photometric data from BYU and from archives as well as how that data is processed. In Chapter 3 we will discuss how we analyzed the data in order to find period solutions and additional pulsational frequencies. Additionally, we will go over the potential pulsational modes for each star and compare them against existing P-L relations. In Chapter 4 we will either reaffirm or question the published classifications and compare the usefulness of each survey in analyzing variable stars. Finally, we will touch on potential future research that could be done to improve our understanding of these objects.

Chapter 2

Observations

All observations made in this project are photometric in nature. The purpose of taking photometric data is to measure the brightness, or apparent magnitude, of a star as it changes over time. This is done using a telescope equipped with a camera which tracks the star across the sky and takes pictures at an exposure time that does not under- or over-expose the star.

2.1 Robotic Observations

Observations were taken for each star at the Orson Pratt Observatory in the Eyring Science Center at BYU, located in Provo, Utah. The data presented in this research comes from the 12-inch telescope for MATLAS 14 and MATLAS 69 and the now-defunct 10-inch telescope for MATLAS 7 and MATLAS 14. The 12-inch telescope is a TPO 12" with a focal length of 2440 mm, while the 10" is a Takahashi Mewlon 250 mm with a focal length of 3000 mm. Images were binned 2×2 and were primarily captured on CCD cameras using the Johnson-Cousins V filter which measures light at 540 nm. There is also minimal data available in the B filter for MATLAS 14. A summary of the data collected from the BYU telescopes is found in Table 2.1. We will primarily be analyzing data in the V filter since it is the most abundant.

Table 2.1. Photometric Observations from BYU

Target	Obs. Start	Obs. End	Nights Observed	Hours Observed	Used Frames (Total)
MATLAS 7	Jul 2019	Aug 2019	13	76.11	814 (842)
MATLAS 14	Mar 2019	May 2023	24	78.79	1350 (1493)
MATLAS 69	Mar 2021	May 2023	12	25.27	352 (384)

All frames were reduced using standard IRAF procedures (Tody 1986). This involves taking multiple calibration frames using the telescope which are then combined and then subtracted from the light frames, which are pictures of the object, in order to reduce noise. We produced light curves from these light frames using AstroImageJ (Collins et al. 2017). This involves selecting comparison stars in the field for which the brightness is well known and stable. Knowing the apparent magnitude of the comparison stars within a specified aperture, AstroImageJ can then calculate the apparent magnitude of the target star for each observation.

A sample field for MATLAS 7 taken on the 10" telescope in the V filter is shown in Figure 2.1. Comparison stars were selected using the SIMBAD database by querying for nearby stars in the field (Wenger et al. 2000) However, there were generally very few stars in any of our image fields which were contained in SIMBAD. To supplement our comparison stars, we use the Aladin interactive sky atlas to find published V magnitude in other surveys (Bonnarel et al. 2000). All of our comparison star magnitudes come from the fourth United States Naval Observatory CCD Astrograph Catalog, UCAC4 (Zacharias et al. 2013). The criteria for selecting comparison stars were that the object is classified as a non-variable star and that it has a published V magnitude within a reasonable range of the target star (i.e., for a given exposure, the comparison star should not be over- or under-exposed). Comparison star positions, magnitudes, and IDs (when available) are given in Table A.1.

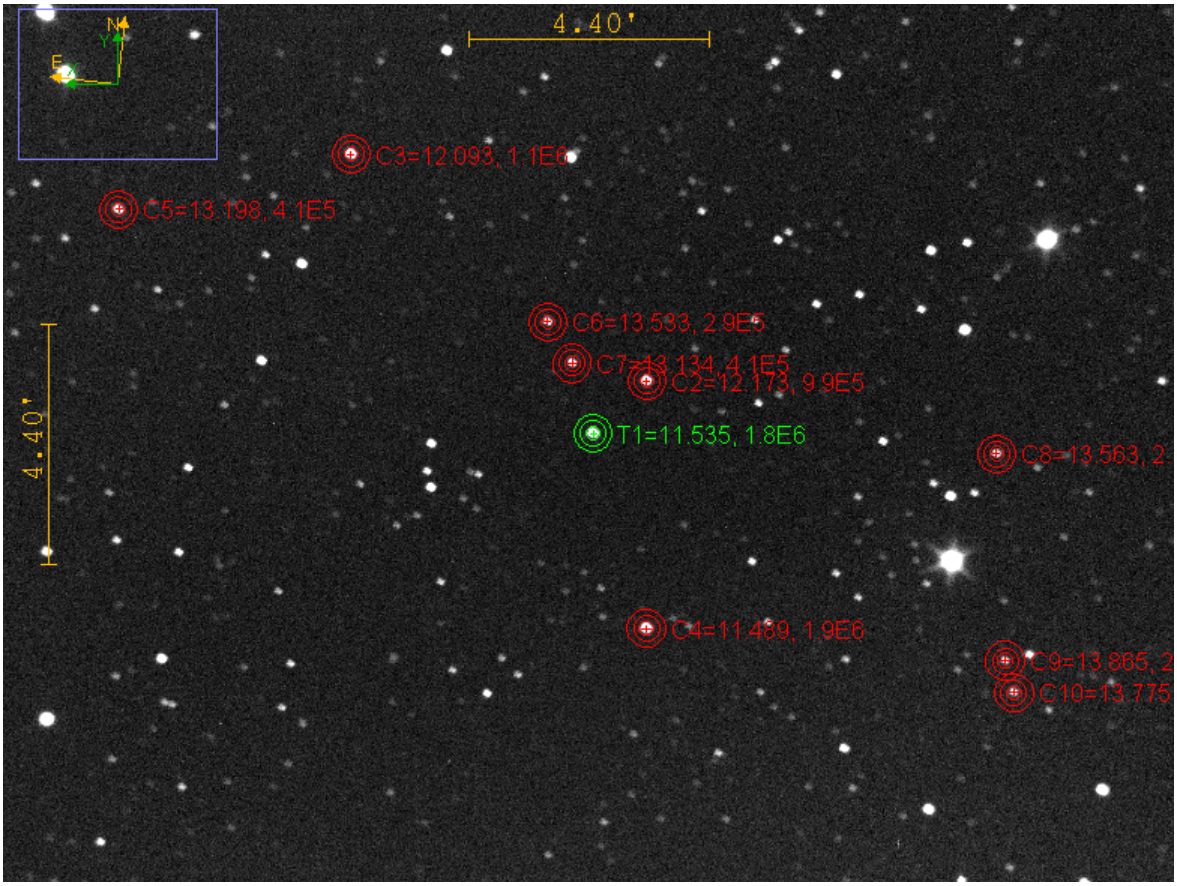

Figure 2.1 Sample field for MATLAS 7 from the 10" telescope at BYU. MATLAS 7 is marked with a green aperture and labeled T1. Comparison stars are marked with red apertures as C2, C3, etc.

Table 2.2. Photometric Observations from ASAS-SN & ATLAS

Target	ASAS-SN g	ASAS-SN V	ATLAS c	ATLAS o
MATLAS 7	2065	1043	123	102
MATLAS 14	1296	729	123	136
MATLAS 69	1790	809	137	136

2.2 Archival Photometry

Additional photometric data was pulled from several different surveys. This data, taken in different filters with different exposures and cadences and at different times, allows us to confirm the periodicity of our targets. Analysis of this data is presented in Section 3.

2.2.1 ATLAS and ASAS-SN

We downloaded light curve data from the ASAS-SN variable star database in both g and V filters (Jayasinghe et al. 2019; 2021). Data from ATLAS came in o and c filters (Heinze et al. 2018). Table 2.2 indicates the number of observations for all objects in each filter. While there is a fair amount of data from ASAS-SN, the time-density of the observations is not high enough to find times of maximum light (see Section 3.1). However, this data can still be used to confirm primary and sometimes secondary frequencies. Unfortunately, the ATLAS data is so sparse that only the primary frequency can be confirmed—if it is resolved at all—in the Fourier decomposition process (see Section 3.2).

Table 2.3. Photometric Observations from TESS

Target	TESS ID	Sector	Exposure (s)	Data Points
MATLAS 7	462349240	54	600	1823
MATLAS 14	21547177	21	1800	1250
		47	600	3735
MATLAS 69	903327435	22	1800	891
		45	600	3238
		46	600	3382
		49	600	2698

2.2.2 TESS

TESS observes a particular sector of the sky continuously for several days at a time (Ricker et al. 2015). Each observation produces a large full-frame image, $24° \times 96°$ in size. As such, each star is only a few pixels in size. However, the star stays on these same pixels throughout the observation period so high-quality light curves can be extracted. The quality of the data is heightened by the fact that TESS is in space, so there is no atmospheric interference causing extra noise.

Older TESS sectors were taken with 30-minute (1800 s) exposures and newer sectors are taken with 10-minute (600 s) exposures.[1] We were able to retrieve data from the Mikulski Archive for Space Telescopes (MAST) portal for all three of our targets. A summary of this data can be found in Table 2.3.

After downloading the data, light curves were extracted using AstroPy (Astropy Collaboration et al. 2013; 2018). Due to the high observation cadence, times of maximum light could easily be

[1]The latest TESS observations are made with 2-minute exposures, but at the time of analysis, there were no fields available for our stars.

extracted using Peranso (Paunzen & Vanmunster 2016). As a result, most times of maximum light we used to calculate the ephemeris and perform O-C analysis for each star in Section 3.1 are from the TESS data.

Chapter 3

Analysis

There are several software tools which we used to analyze the abundance of photometric data for each star. We calculated the primary period of each star in Section 3.1. We then determined whether each star was multiperiodic using the methods in Section 3.2.

3.1 Times of Maximum Light

We used Peranso (Paunzen & Vanmunster 2016) to obtain times of maximum light from the BYU data and the TESS data for all three stars. This was done by fitting a fifth-order polynomial to the data surrounding each observed maximum. Using these maxima, we then determined an ephemeris for each object, shown in Table 3.1. An ephemeris equation is a line fitted to the times of maximum observed for each cycle of pulsation. The slope of the line is the period in days and the intercept is the time of maximum for an arbitrarily picked starting cycle, usually the first maximum observed. Since MATLAS 69 is classified as an eclipsing binary, we found the primary minima instead of the maxima.

Now, armed with our ephemeris equations, we were able to calculate the phase in the pulsation cycle for all the data points in each survey. The results are phased light curves which show us what

Table 3.1. Ephemeris from Times of Maximum Light

Target	No. Maxima/Primary Minima	Ephemeris
MATLAS 7	235	$HJD_{max} = 2458675.813(72) + 0.06581768(34)E$
MATLAS 14	247	$HJD_{max} = 2459302.761(29) + 0.198455(92)E$
MATLAS 69	244	$HJD_{max} = 2458902.006(31) + 0.3284687(04)E$

the pulsation shapes are for each star. By visual inspection, we can begin to determine some of a star's characteristics.

For example, Figure 3.1 compares the phase diagrams for the BYU data as well as each archival survey, separated by filter. We can see that the pulsation shape matches in each survey and that the data phase well with the calculated period. MATLAS 7 already appears to be multiperiodic because its light curve is not thin enough to be represented by a single sine wave. There must be at least one additional frequency causing the shape to vary, which we determine in Section 3.2. Lastly, we can easily compare the amount and quality of data in each survey based on the density and scatter of the curves. We compare the surveys in detail in Section 4.1.

There is somewhat more archival data available for MATLAS 14, whose phased light curves are shown in Figure 3.2. We were also able to observe in the *B* filter as well as the *V* at BYU. Unlike MATLAS 7, for which the BYU observations are contained within a single summer, we obtained our photometric data for MATLAS 14 in multiple seasons with long breaks between observations. There tend to be apparent magnitude differences between observation periods, causing the BYU light curve to appear thicker than it should be. ASAS-SN data suffers from a similar problem in addition to higher measurement errors, both contributing to a messy-looking light curve. The TESS curves are closer to what the variation should actually look like.

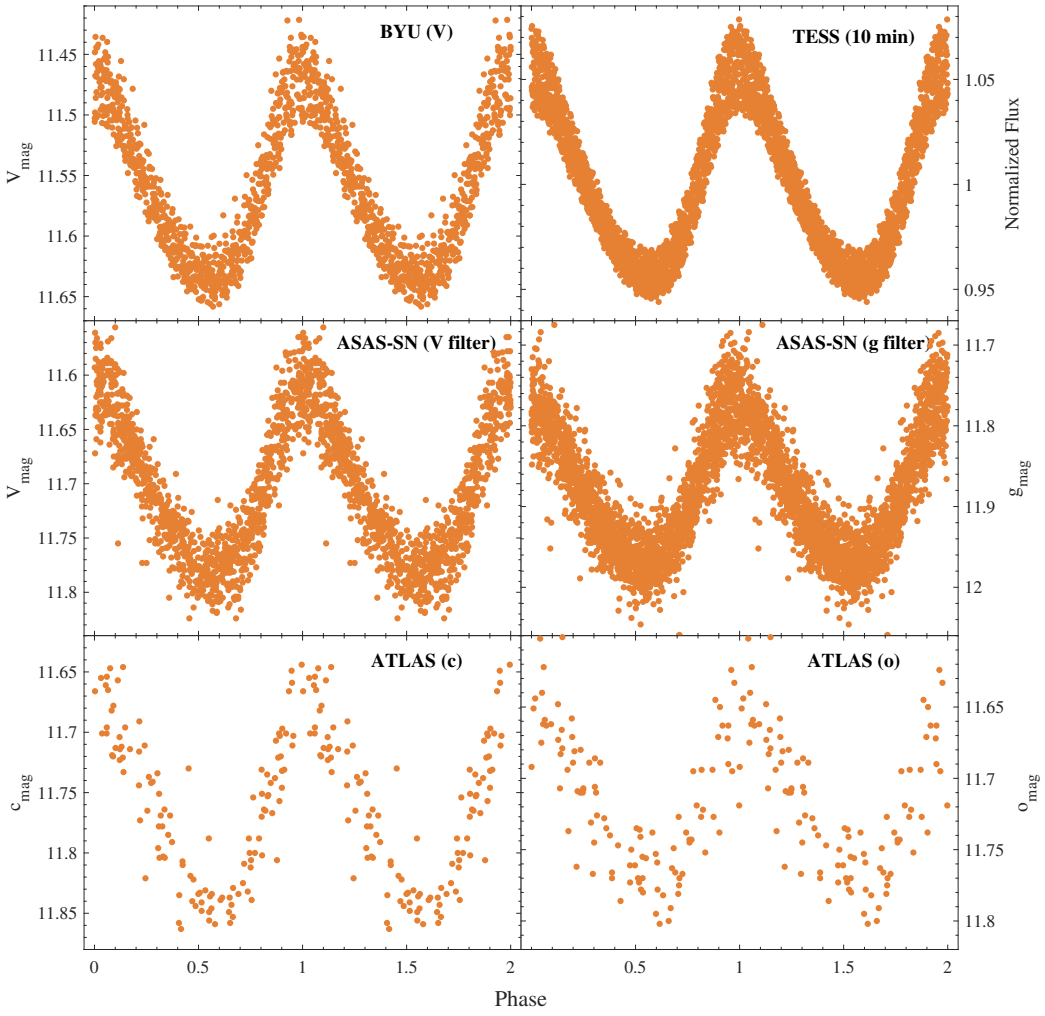

Figure 3.1 Phased light curves for MATLAS 7 from each survey. These light curves are phased with double the period so as to better show the pulsation shape.

It is immediately apparent that MATLAS 14's curves look like sine waves, causing us to doubt whether it is actually multiperiodic. Although there is some thickness that could be attributed to multiperiodicity, it is more likely due to the observing issues described. If we unfold a TESS light curve to look at individual variations for single cycles, we see that MATLAS 14 appears to vary similarly to MATLAS 69, with minima of alternating depths. This is one of our first clues that MATLAS 14 may actually be a WUma binary rather than a δ Scuti star. Another tell is that the brightness of MATLAS 14 changes at the same rate for both the rise and fall of the cycle. In contrast, MATLAS 7 brightens faster than it dims, causing the slant to its light curves in Figure 3.1. This type of shape is typical for most variable stars.

The light curves for MATLAS 69 are shown phased with double the binary period in Figure 3.3. Since MATLAS 69 is an eclipsing binary, its period includes both minima. Thus, phasing with double the period produces a light curve with four minima. It is difficult to see the different eclipse depths in the BYU and ATLAS data because of the limited number of observations, and in the ASAS-SN data because of the scatter. However, the 30-minute exposure TESS data clearly shows this feature.

The process of finding primary minima for MATLAS 69 in order to determine the ephemeris was complicated by the fact that the eclipse depths in its light curve appear to vary over time. Looking at the 10-minute TESS light curve, the variation is apparent in relative thickness of the minima and maxima in comparison with the rest of the curve. Since the two stars of a WUma system are in contact with each other, this may be due to them exchanging mass with each other. A process such as this would cause one star to become slightly brighter while the other becomes slightly dimmer, which changes the shape of the light curve over time. A similar phenomenon occurs for MATLAS 14 and is also visible in its TESS curves in Figure 3.2.

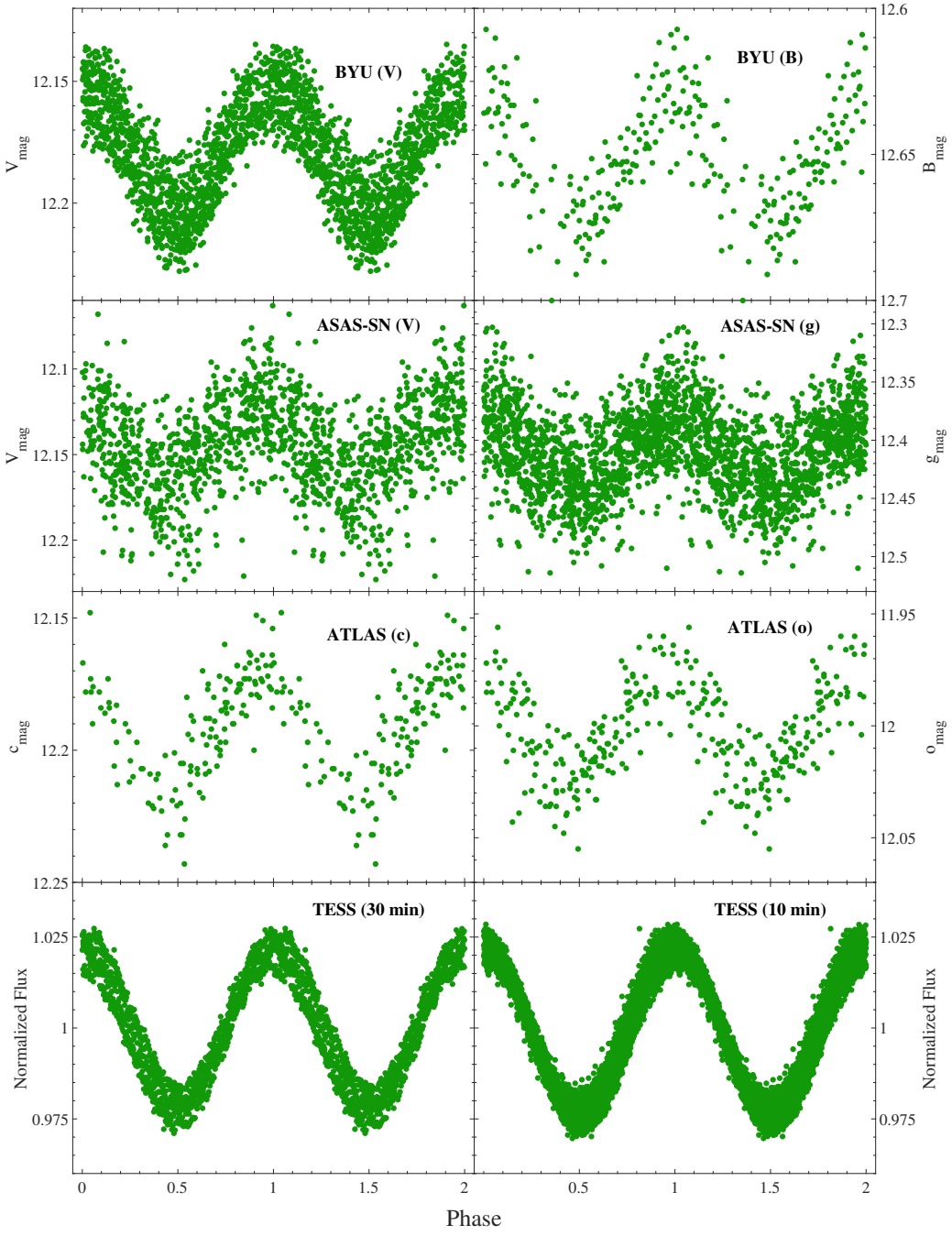

Figure 3.2 Phased light curves for MATLAS 14 from each survey. These light curves are phased with double the period so as to better show the pulsation shape.

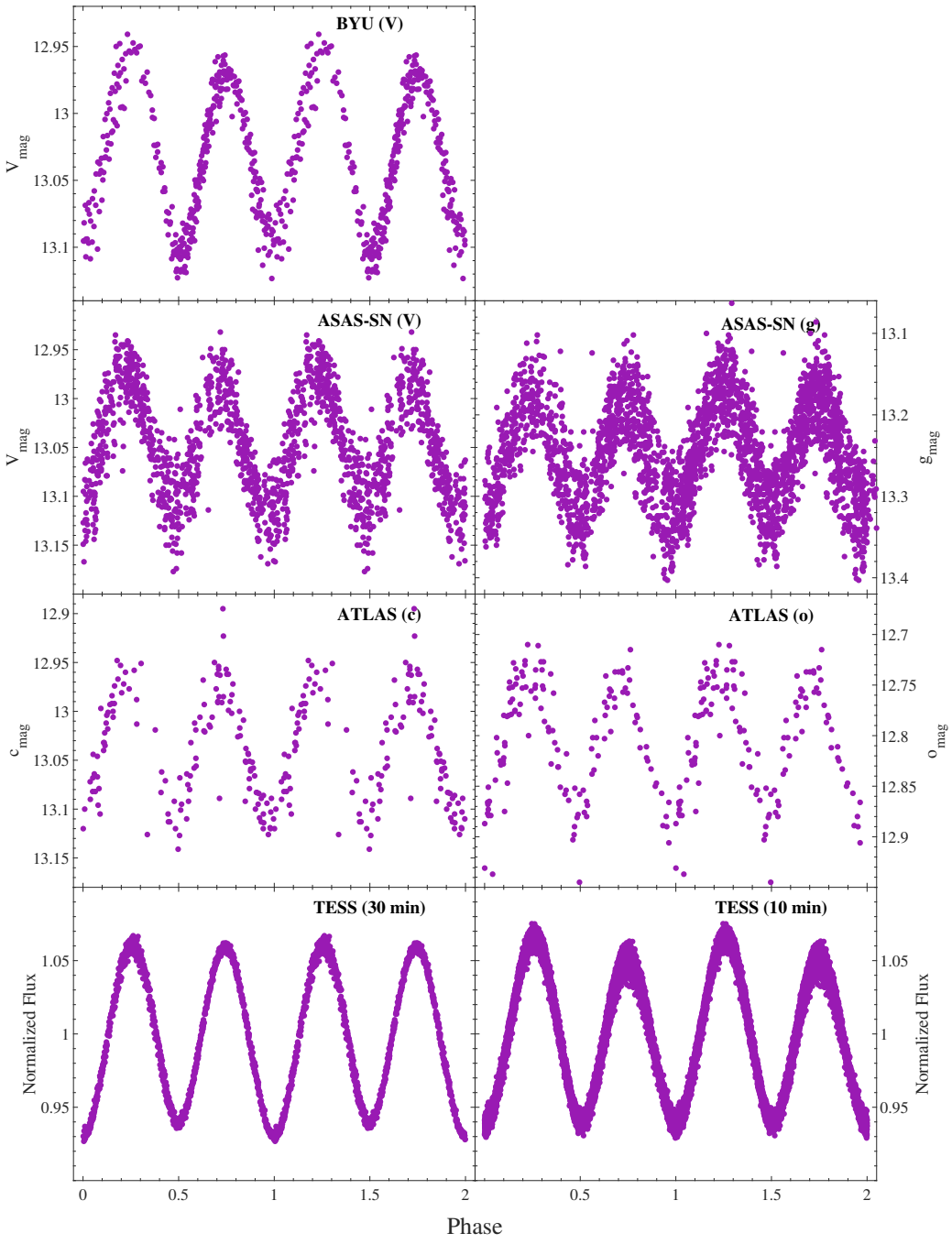

Figure 3.3 Phased light curves for MATLAS 69 from each survey. These light curves are phased with double the period.

3.1.1 O-C Analysis

The purpose of observed minus calculated (O-C) analysis is to find whether the period of a star's pulsation changes over time. Using our newly-derived ephemeris equations, we calculated times of maximum (or minimum) light for each cycle during which we observed a maximum (or minimum). Subtracting those times from the observed times allowed us to create O-C graphs for each star.

We can see in Figure 3.4 that there is no significant change in the period of MATLAS 7 since the O-C values are near zero for an extended time frame (nearly 20,000 cycles); if there were a period change, the graph would have a slope. The O-C diagram for MATLAS 14 in Figure 3.5 has an interesting shape, which may be due to its binary nature, as the distance between the two stars causes their brightness to be measured at slightly different times. However, there is no overall slope to the O-C so there appears to be no change in period. There appears to be some slope in the O-C for MATLAS 69 as seen in Figure 3.6. Since the variation is near zero, and MATLAS 69 is not observed over a long enough time frame, nothing can be said about its change in period for the long term.

3.2 Fourier Decomposition

We performed Fourier analysis using Period04 (Lenz & Breger 2005) on all data sets in order to determine the multiperiodicity of our stars. This involves using Fourier transforms to decompose the time domain data into various sine waves, whose frequencies and amplitudes are analogous to the star's pulsation frequencies and amplitudes. Here we summarize some of the significant results. Due to their length, all tables of extracted frequencies referenced in this section are included in Appendix A. Some resulting frequencies were eliminated from the tables due to similarity to observation cadence/Earth rotation or low signal-to-noise ratio (SNR).

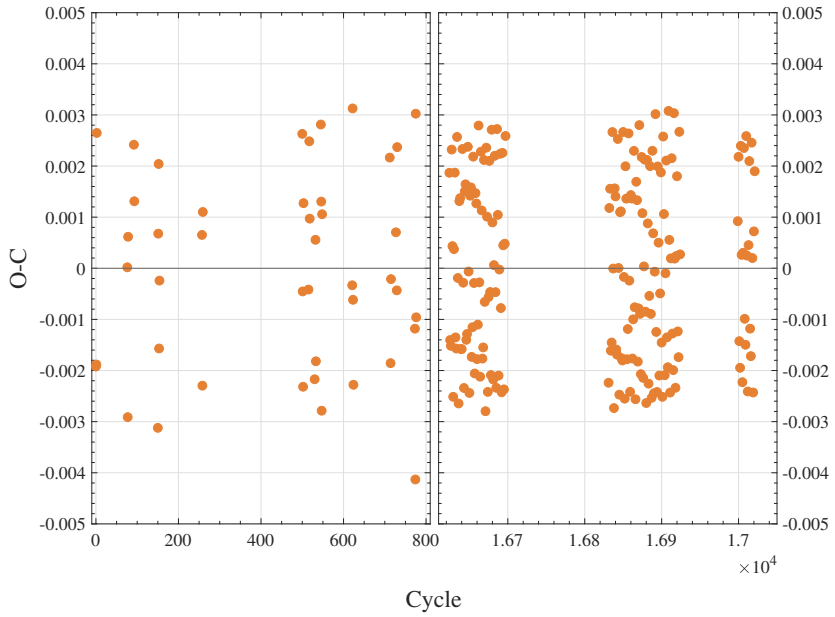

Figure 3.4 Observed minus calculated times of maximum light for MATLAS 7.

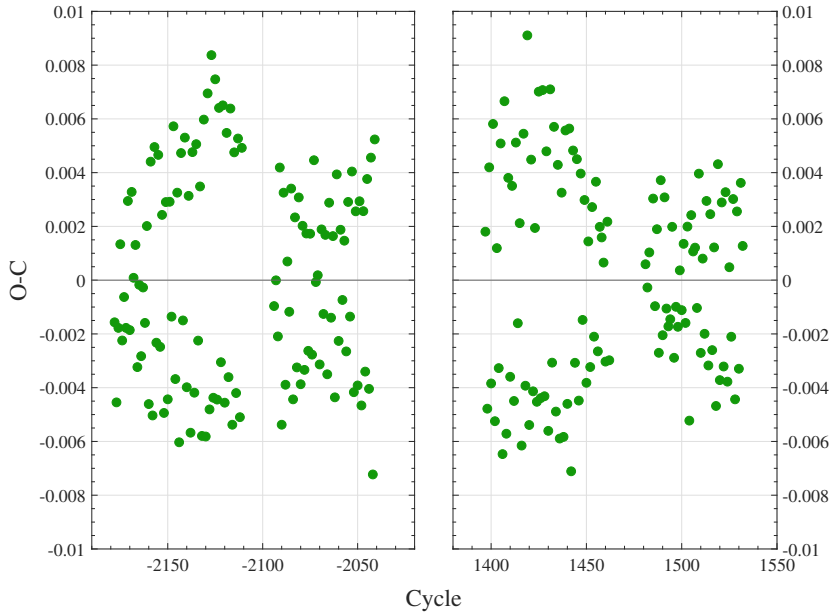

Figure 3.5 Observed minus calculated times of maximum light for MATLAS 14.

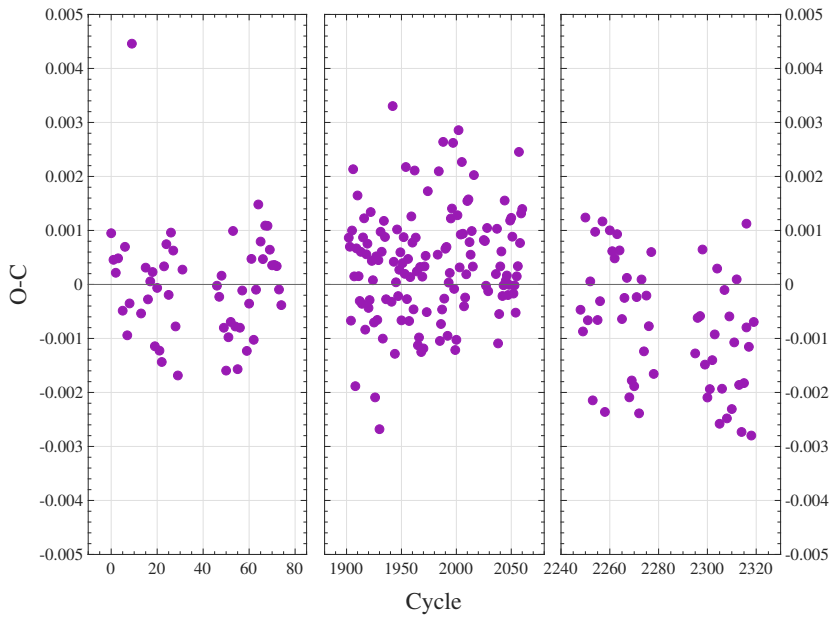

Figure 3.6 Observed minus calculated times of maximum light for MATLAS 69.

In all surveys except the ATLAS c filter, the primary frequency for MATLAS 7 agrees well with the published period. MATLAS 7 appears to be multiperiodic, with a primary frequency of 15.193 c/d and a secondary frequency of 19.556 c/d found in multiple sets of data with different filters, exposures, and observation cadences. Notice also that in Table A.2 several combinations and multiples of these two frequencies are found, which further confirms that these are real pulsational frequencies. These frequency peaks can be easily identified in the Fourier spectra, shown in Figure 3.7.

All primary frequencies found for MATLAS 14 and shown in Table A.3 agree with the published period. None of the Fourier analyses were able to find multiples of f_1 but found some frequencies close to (but not quite) $0.5 f_1$. It is therefore possible that this star is pulsating in the first harmonic. A more likely possibility is that MATLAS 14 is an eclipsing binary similar to MATLAS 69, since the Fourier decompositions for these two stars are highly similar. Its Fourier spectra are shown in Figure 3.8.

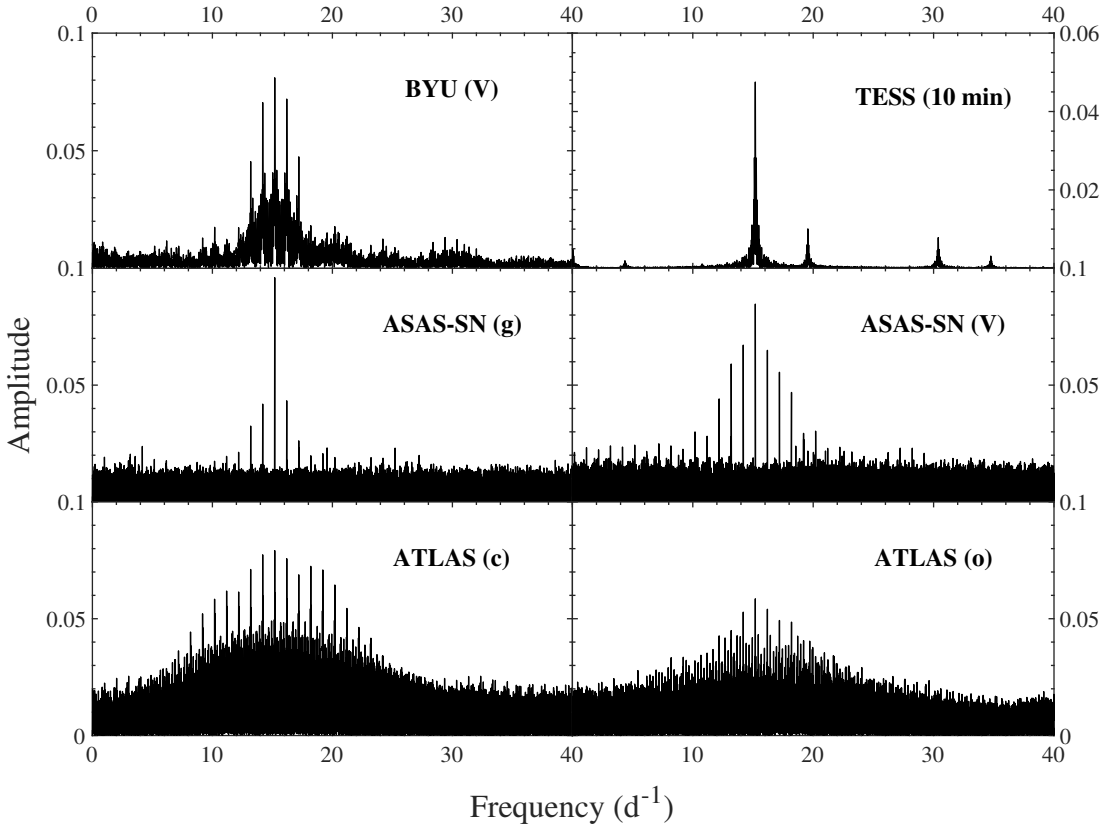

Figure 3.7 Fourier spectra for MATLAS 7 from each survey.

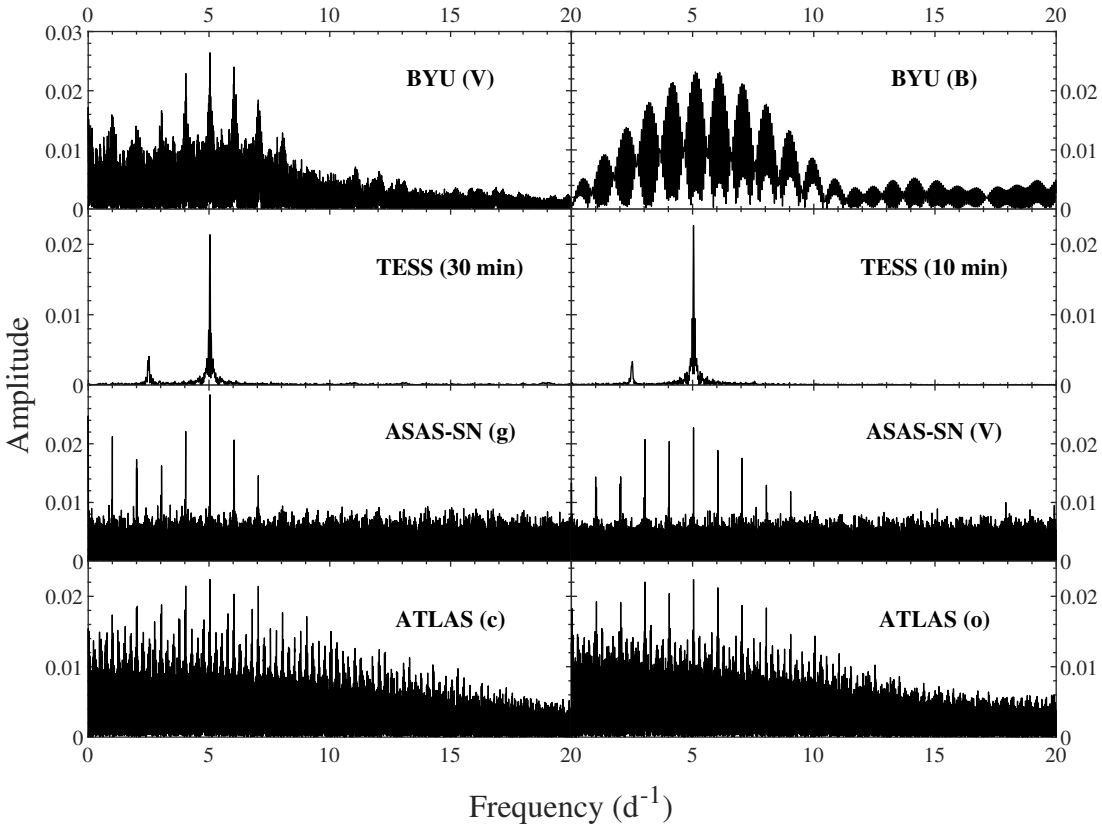

Figure 3.8 Fourier spectra for MATLAS 14 from each survey.

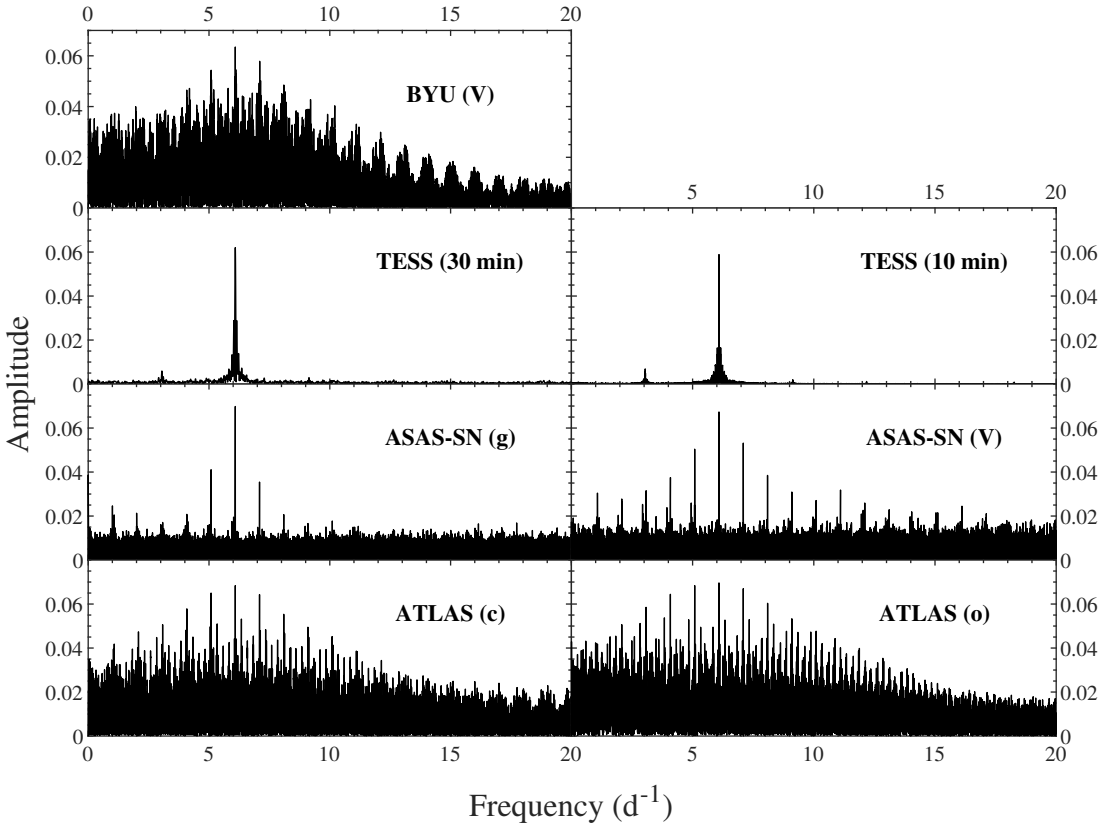

Figure 3.9 Fourier spectra for MATLAS 69 from each survey.

The major frequency f_1 for MATLAS 69 found in each survey in Table A.4 was twice that of the published frequency from ASAS-SN. In most surveys, after some prewhitening, $0.5f_1$ is recovered, then $1.5f_1$, then $2f_1$, etc. This is characteristic of a Fourier spectrum for a W Ursae Majoris star, where the real frequency is $0.5f_1$ but the similarity of the light curve to a pulsating star causes twice the real frequency to be extracted first. Its Fourier spectra, shown in Figure 3.9, are very similar to the spectra for MATLAS 14 in Figure 3.8.

Table 3.2. Quantities used to calculate the pulsation constant Q

Object	P (d)	$\log g$ (cm/s^2)	M_{bol}	T_{eff}	Q
MATLAS 7	0.065818	4.0	1.996	7370	0.027
MATLAS 14	0.198456	3.7	2.074	6100	0.049
MATLAS 69	0.082117	4.3	4.122	5920	0.062

3.3 Pulsation Modes

Similar to acoustic waves, gravitational waves in stellar interiors can pulsate in different modes. For example, a star can be pulsating in the fundamental frequency, or it could be pulsating in the first, second, or even higher harmonics. Modes can also be radial or non-radial. HADS have radial modes in the fundamental, first, or second harmonic. Non-radial pulsators tend to have much lower amplitudes (Breger 1990). To aid in identifying these modes, we can calculate the pulsation constant Q using the following formula (Breger & Bregman 1975):

$$\log Q = -6.454 + \log P + 0.5 \log g + 0.1 M_{bol} + \log T_{eff} \tag{3.1}$$

where P is the period in days, g is the surface gravity in cm/s^2, M_{bol} is the absolute bolometric magnitude, and T_{eff} is the effective surface temperature of the star in Kelvin. We obtained g and T_{eff} values from Gaia Data Release 3 (DR3) (Gaia Collaboration et al. 2016; 2023). Our P values were calculated in Section 3.1; in this section we treat MATLAS 69 as if it were a pulsator by using half of the calculated binary period. M_{bol} was obtained by subtracting a bolometric correction of 0.08 from the average absolute magnitude of each star, calculated using Equation 3.2. All of these quantities are provided in Table 3.2 along with our calculated Q values.

The value of Q for MATLAS 7 is fairly typical of a fundamental radial pulsator (Breger 2000). However, the Q values for MATLAS 14 and MATLAS 69 lie outside the range for pulsators, even

when allowing a generous 20% error due to uncertainties in distance, g, and T_{eff} measurements. It is important to note that the pulsation constant is only one metric, and that it must be used in conjunction with other data to confirm stellar pulsation modes.

In Section 3.2, we found that MATLAS 7 is pulsating with two frequencies, $f_1 = 15.193$ c/d and $f_2 = 19.556$ c/d. The ratio f_1/f_2 is 0.7769, which is typical of a fundamental pulsator with two modes that is oscillating radially (Breger 2000). We only identified one pulsation mode for MATLAS 14 and MATLAS 69. The fact that we extracted half of the first frequency before double the first frequency for both of these stars could mean that they are first overtone pulsators. This is in contrast with MATLAS 7, where we extract double the first frequency. However, this type of frequency spectrum is also typical of an eclipsing binary with similar eclipse depths.

3.4 The Period-Luminosity Relation

As discussed in Chapter 1, δ Scuti stars obey a P-L relation which can be used to determine the distance to a star knowing its period and apparent magnitude. Since we have distance measurements available from Gaia DR3 (Gaia Collaboration et al. 2023) and stellar extinction measurements from GALExtin (Amôres et al. 2021), we are able to work backwards and calculate the luminosity in the form of absolute magnitude. This is done using a form of the distance modulus equation:

$$M_V = V - 5\log d + 5 - A_V \tag{3.2}$$

where V is the average apparent visual magnitude, d is the distance to the star in parsecs (pc), A_V is the extinction in the V band caused by interstellar gas and dust obscuring some of the light, and M_V is the absolute visual magnitude. All values used in Equation 3.2 are shown in Table 3.3.

We plotted MATLAS 7 and MATLAS 14 against the δ Scuti P-L relations in Figure 3.10. It is obvious that while MATLAS 7 fits the fundamental P-L relation very well, MATLAS 14 does

Table 3.3. Quantities used in calculating absolute visual magnitude

Object	V	d (pc)	A_V	M_V
MATLAS 7	11.561898	704	0.248	2.076
MATLAS 14	12.186544	899	0.264	2.154
MATLAS 69	13.035646	561	0.089	4.202

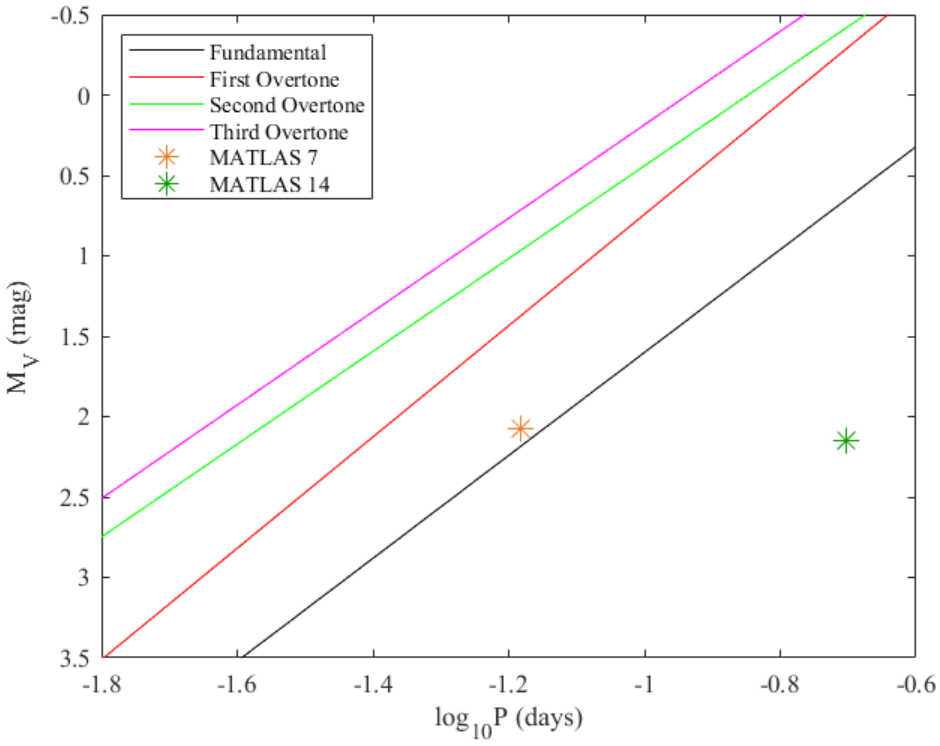

Figure 3.10 Period-luminosity relation for δ Scuti stars. MATLAS 7 and MATLAS 14 are plotted against the P-L relations defined in (Poro et al. 2021).

not. This could either mean that the P-L relations are flawed, or more likely, that MATLAS 14 is classified incorrectly.

Chapter 4

Conclusions

We agree with ATLAS's classification of MATLAS 7 as a pulsating variable star and also with ASAS-SN's classification of it as a HADS. We further find it to be a double-mode fundamental radial pulsator. In contrast, we disagree with ATLAS classifying both MATLAS 14 and MATLAS 69 as pulsating variable stars. We believe that MATLAS 69 is a WUma as designated by ASAS-SN, and that MATLAS 14 is also a star of this type as opposed to a δ Scuti. This raises questions about the current accuracy of machine learning in classifying variable stars, and brings up the need for independent researchers to check these designations for themselves by analyzing and comparing different data sets.

4.1 Survey Utility

Multiple data sets were used in this research, each with their own strengths and weaknesses. The usefulness of photometric data is highly dependent on the noise, which results from atmospheric interference, exposure times, observation frequency, inferior equipment, and sometimes just a lack of sufficient data. Additionally, some observation bands are more useful than others because researchers' preference of them in the past influenced the types of calculations and equations used

to analyze objects. One aim of this project was to determine how useful different types of surveys are for variable star research. In Chapter 3 we compared the surveys using phased light curves (Figures 3.1, 3.2 and 3.3) and Fourier spectra (Figures 3.7, 3.8, and 3.9). In this section we shall summarize the pros and cons of using each dataset that we found in our analysis.

4.1.1 BYU

Here we use BYU as a stand-in for independent ground-based telescopes. If researchers have access to their own research telescopes, they can choose which objects to study rather than relying on the availability of archival data or competing with other proposals for telescope time. We were able to choose the proper telescope and exposure time to best measure our target stars. We also use the common V band filter and can choose to measure in other filters such as B to compare. We were able to observe our objects over multiple nights to obtain the amount of data we needed.

There are certainly limitations to using these ground-based telescopes. Although we process our data to reduce noise, some atmospheric interference can never be subtracted out, and the entire process is tedious. Observations can only be made at night under ideal conditions; especially in winter, this time is limited. Additionally, the telescopes must perform a meridian flip to continue recording data when stars cross from east to west, which can cause a jump in the data. Ideally, stars should stay at the same positions on the frame since different CCD pixels have different measuring capabilities. Unfortunately, telescope tracking is not always accurate and stars can drift or "smear" across the frame. We can get an idea of how bad these problems are from the size of the errors in magnitude. Larger telescopes such as the 12-inch observe more accurately than smaller telescopes.

Despite these problems, our observations are still valuable for analyzing these stars. We are able to obtain a lot of closely-spaced data from which we can extract times of maximum light. Aliasing problems in the Fourier analysis are also reduced (except for the common 1 c/d which arises from observation frequency).

4.1.2 ATLAS and ASAS-SN

ATLAS is a large-scale survey, and as such, it has data on numerous targets. However, the number of data points per target is limited and spread out over a long observing period. Thus, only the primary frequency can be extracted with Fourier analysis, but it is not always accurate, as the SNR is low. ATLAS observes in the *c* (cyan) and *o* (orange) bands which are in the visible spectrum but not the same as the common *V*. ATLAS cannot always be relied on for accurate classifications and should only be used in conjunction with other surveys.

ASAS-SN has significantly more data than ATLAS and its classifications are more specific. Sometimes, frequencies beyond the primary can be extracted, but the SNR is still low, since the data points are spread out over time. Like ATLAS, it is a survey using ground-based telescopes and suffers from some of the same problems as the BYU data. It does observe in the useful *V* band as well as *g* (green). Again, its classification system cannot be completely relied upon. It must also be used in conjunction with other surveys.

4.1.3 TESS

Since TESS observes in space, there is no atmospheric interference. The fields are large, meaning each target is only a few pixels, but the tracking is so sophisticated that the stars remain on the same few pixels for most of each observing period, making measurements highly accurate. The SNR is very low both because of this and because TESS observes continuously for a long period with exposure times of 30 minutes or less. TESS data is excellent for finding times of maximum light, allowing for accurate period solutions. Additionally, several frequencies can be extracted with high SNR.

One downside of TESS is that it observes in its own broadband filter, meaning the data cannot be magnitude solved and cross-compared in that way; only the stellar flux can be measured. Sometimes the sun appears in the field and interferes with observation by causing large errors in measured flux.

However, the importance of TESS in this type of research cannot be overstated as it has been used in many projects similar to ours. The ability to find many frequencies allows for more detailed asteroseismology work.

4.2 Future Work

The research of multiperiodic variable stars at BYU is ongoing, with several papers to be published in the near future. More work is needed to confirm the classifications of MATLAS 14 and MATLAS 69 so that the discrepancies can be suitably resolved. MATLAS 7 serves as a good example of a HADS which can be used to identify similar objects.

The results of our work warn that the classifications produced by machine learning algorithms are not always reliable. We advise other researches to do their own analysis of the data, relying on multiple surveys and archival measurements to provide a fuller picture of the behavior of variable stars.

Appendix A

Additional Tables

Table A.1. List of comparison stars used with the BYU photometry

Target (T1)	#	Identifier	Right Ascension	Declination	V_{mag}
MATLAS 7	C2	—	20:19:22.030	+10:07:56.51	12.173
	C3	—	20:19:39.639	+10:13:31.70	12.348
	C4	TYC 1078-824-1	20:19:45.851	+10:11:26.55	12.093
	C5	—	20:19:48.530	+10:09:20.21	12.245
	C6	—	20:19:50.665	+10:07:29.43	12.716
	C7	TYC 1078-256-1	20:19:29.554	+10:11:50.45	11.756
	C8	—	20:19:37.394	+10:06:20.48	12.868
	C9	—	20:19:37.047	+10:05:32.64	12.545
	C10	—	20:19:55.463	+10:01:51.17	12.340
	C11	—	20:20:04.898	+10:03:33.52	12.768
	C12	TYC 1078-1229-1	20:18:58.930	+10:09:32.16	11.690
	C13	UCAC2 35479650	20:18:58.548	+10:06:28.93	12.315
	C14	TYC 1078-1355-1	20:19:19.921	+10:03:26.21	11.489
	C15	—	20:18:57.494	+10:00:44.32	11.986
	C16	TYC 1078-1398-1	20:18:44.837	+10:01:27.66	11.507
MATLAS 14	C2	—	08:55:51.331	+42:47:22.09	12.813
	C3	—	08:56:37.510	+42:52:51.53	12.509
	C4	TYC 2989-160-1	08:56:51.766	+42:52:16.95	12.099
	C5	—	08:56:43.380	+42:41:39.54	12.632
	C6	—	08:56:14.985	+42:40:04.33	11.921
	C7	TYC 2989-384-1	08:55:28.145	+42:51:52.62	11.364
	C8	—	08:55:11.397	+42:53:52.27	12.648
	C9	—	08:55:29.100	+42:53:54.60	12.634
MATLAS 69	C2	—	11:51:29.351	+10:23:22.32	14.056

Table A.1 (cont'd)

Target (T1)	#	Identifier	Right Ascension	Declination	V_{mag}
	C3	—	11:51:21.641	+10:24:15.96	12.854
	C4	—	11:51:48.436	+10:10:30.51	12.491
	C5	TYC 867-623-1	11:51:06.096	+10:13:15.58	11.731
	C6	—	11:51:02.658	+10:12:39.24	12.594
	C7	TYC 867-962-1	11:50:47.375	+10:09:59.13	11.706

Note. — Stars without identifiers have no entry in SIMBAD but can be found in other databases such as UCAC4 with position data. All V_{mag} values come from UCAC4 (Zacharias et al. 2013).

Table A.2. MATLAS 7 frequencies calculated using Period04

Survey	Order	Frequency (c/d)	Amplitude	SNR
Published	f_1	15.19352756	0.18	-
BYU (V)	f_1	15.19349704	0.0813395649	187.84227
	f_2	19.55630604	0.0179388228	44.54381
	$f_3 = 2f_1$	30.38699408	0.0131563320	71.85975
	$f_6 = f_1 + f_2$	34.74882443	0.0045234277	19.46910
	$f_9 = f_2 - f_1$	4.36085171	0.0026998385	6.10313
ASAS-SN (g)	f_1	15.19351517	0.0964195192	98.73178
	f_2	19.55641296	0.0215661534	22.34023
	$f_4 = 2f_1$	30.38700217	0.0142507558	14.70466
	$f_6 = f_1 + f_2$	34.74992613	0.0066757660	6.58622
ASAS-SN (V)	f_1	15.19348209	0.0830641424	63.12746
	f_2	19.55641392	0.0162609390	12.25251
	$f_3 = 2f_1$	30.38698484	0.0129907622	9.87599
ATLAS (c)	f_1	14.19082341	0.0809639924	32.02231
ATLAS (o)	f_1	15.19344040	0.0587329041	24.13486
TESS (10 min)	f_1	15.19320739	0.0475832210	385.70696
	f_2	19.55701087	0.0099556859	139.07698
	$f_3 = 2f_1$	30.38641478	0.0079062628	122.74139
	$f_5 = f_1 + f_2$	34.75021826	0.0030654506	66.49193
	$f_6 = f_2 - f_1$	4.36189622	0.0020938252	32.19738
	$f_8 = 3f_1$	45.57962217	0.0013275566	27.08515

Table A.3. MATLAS 14 frequencies calculated using Period04

Survey	Order	Frequency (c/d)	Amplitude	SNR
Published	f_1	5.03882922	0.07	-
BYU (V)	f_1	5.03889845	0.0249499522	85.76888
	$f_4 = 0.5f_1$	2.51961263	0.0029535932	11.46695
BYU (B)	f_1	5.11704978	0.0219165808	22.35830
ASAS-SN (g)	f_1	5.03891008	0.0270557389	18.62187
ASAS-SN (V)	f_1	5.03879114	0.0232640173	18.21326
ATLAS (c)	f_1	5.03875162	0.0245229266	20.81698
ATLAS (o)	f_1	5.03874251	0.0226478186	17.69754
TESS (30 min)	f_1	5.03807031	0.0212105445	391.89695
	$f_2 = 0.5f_1$	2.51720446	0.0037785355	51.66601
	f_3	2.47509850	0.0031496143	42.41766
	$f_6 = 1.5f_1$	7.55893617	0.0004100019	9.14729
TESS (10 min)	f_1	5.03825561	0.0223921553	288.21296
	$f_2 = 0.5f_1$	2.51359936	0.0031538852	28.95086
	f_3	2.48227151	0.0023857729	21.82153
	$f_5 = 1.5f_1$	7.55738342	0.0006494361	11.87968

Table A.4. MATLAS 69 frequencies calculated using Period04

Survey	Order	Frequency (c/d)	Amplitude	SNR
Published	f_1	3.04441713	0.15	-
BYU (V)	f_1	6.08888928	0.0686059773	139.25493
ASAS-SN (g)	f_1	6.08883147	0.0699926516	59.33920
	$f_4 = 0.5f_1$	3.04444532	0.0103340362	8.60898
ASAS-SN (V)	f_1	6.08881731	0.0689344510	46.41761
	$f_4 = 0.5f_1$	3.04433806	0.0079101182	5.33550
ATLAS (c)	f_1	6.08881751	0.0692726611	37.68203
ATLAS (o)	f_1	6.08883502	0.0700769968	24.19735
TESS (30 min)	f_1	6.08830125	0.0616222103	502.73248
	$f_2 = 0.5f_1$	3.04821491	0.0060360453	45.39076
	$f_4 = 1.5f_1$	9.13245187	0.0017220322	20.01254
	$f_7 = 2f_1$	12.17660250	0.0009055474	11.02449
	$f_{10} = 3f_1$	18.26490375	0.0007148177	8.09315
TESS (10 min)	f_1	6.08868270	0.0582663279	913.69527
	$f_2 = 0.5f_1$	3.04507001	0.0082603130	92.46529
	$f_5 = 1.5f_1$	9.13338838	0.0019237350	40.40547
	$f_8 = 2f_1$	12.17772974	0.0010029883	23.02128
	$f_9 = 3f_1$	18.26677677	0.0008115003	20.41513

Bibliography

Amôres, E. B., et al. 2021, MNRAS, 508, 1788

Astropy Collaboration et al. 2013, A&A, 558, A33

—. 2018, AJ, 156, 123

Bonnarel, F., et al. 2000, A&AS, 143, 33

Breger, M. 1990, in Astronomical Society of the Pacific Conference Series, Vol. 11, Confrontation Between Stellar Pulsation and Evolution, ed. C. Cacciari & G. Clementini, 263–273

Breger, M. 2000, in Astronomical Society of the Pacific Conference Series, Vol. 210, Delta Scuti and Related Stars, ed. M. Breger & M. Montgomery, 3

Breger, M., & Beichbuchner, F. 1996, A&A, 313, 851

Breger, M., & Bregman, J. N. 1975, ApJ, 200, 343

Collins, K. A., Kielkopf, J. F., Stassun, K. G., & Hessman, F. V. 2017, AJ, 153, 77

Gaia Collaboration et al. 2016, A&A, 595, A1

—. 2023, A&A, 674, A1

Heinze, A. N., et al. 2018, AJ, 156, 241

Jayasinghe, T., et al. 2019, MNRAS, 486, 1907

—. 2021, MNRAS, 503, 200

Leavitt, H. S., & Pickering, E. C. 1912, Harvard College Observatory Circular, 173, 1

Lenz, P., & Breger, M. 2005, Communications in Asteroseismology, 146, 53

Lucy, L. B. 1968, ApJ, 151, 1123

Paunzen, E., & Vanmunster, T. 2016, Astronomische Nachrichten, 337, 239

Poro, A., et al. 2021, PASP, 133, 084201

Ricker, G. R., et al. 2015, Journal of Astronomical Telescopes, Instruments, and Systems, 1, 014003

Shappee, B. J., et al. 2014, ApJ, 788, 48

Tody, D. 1986, in Society of Photo-Optical Instrumentation Engineers (SPIE) Conference Series, Vol. 627, Instrumentation in astronomy VI, ed. D. L. Crawford, 733

Wenger, M., et al. 2000, A&AS, 143, 9

Zacharias, N., Finch, C. T., Girard, T. M., Henden, A., Bartlett, J. L., Monet, D. G., & Zacharias, M. I. 2013, AJ, 145, 44

Index